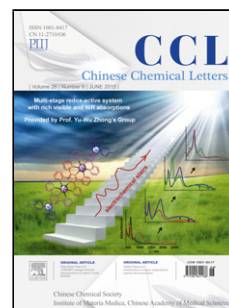


Accepted Manuscript

Title: Macrocyclic *versus* acyclic preorganization in organoplatinum(II)-based host-guest complexes

Authors: Xiaolong Zhang, Yifei Han, Guangyao Liu, Feng Wang



PII: S1001-8417(19)30253-0
DOI: <https://doi.org/10.1016/j.ccllet.2019.05.007>
Reference: CCLET 4975

To appear in: *Chinese Chemical Letters*

Please cite this article as: Zhang X, Han Y, Liu G, Wang F, Macrocyclic *versus* acyclic preorganization in organoplatinum(II)-based host-guest complexes, *Chinese Chemical Letters* (2019), <https://doi.org/10.1016/j.ccllet.2019.05.007>

This is a PDF file of an unedited manuscript that has been accepted for publication. As a service to our customers we are providing this early version of the manuscript. The manuscript will undergo copyediting, typesetting, and review of the resulting proof before it is published in its final form. Please note that during the production process errors may be discovered which could affect the content, and all legal disclaimers that apply to the journal pertain.

Communication

Macrocyclic *versus* acyclic preorganization in organoplatinum(II)-based host–guest complexes

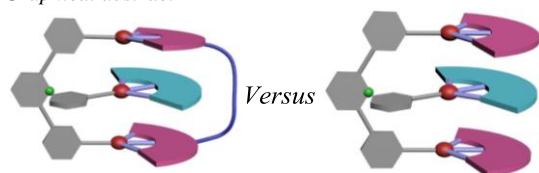
Xiaolong Zhang, Yifei Han, Guangyao Liu, Feng Wang*

CAS Key Laboratory of Soft Matter Chemistry, iChEM (Collaborative Innovation Center of Chemistry for Energy Materials), Department of Polymer Science and Engineering, University of Science and Technology of China, Hefei 230026, China

* Corresponding author.

E-mail address: drfwang@ustc.edu.cn

Graphical abstract



Discrepancy in

- Numbers of Pt---Pt metal-metal bond
- Non-covalent binding affinity
- Photosensitization capability

Two host–guest systems have been constructed, by employing structurally similar terpyridine platinum(II) macrocycle and molecular tweezer as the synthetic receptors. The macrocycle/guest complex displays low-energy emission signal, reinforced non-covalent binding affinity, and enhanced photosensitization capability than those of the molecular tweezer/guest one. The discrepancy between macrocyclic and acyclic preorganization modes originates from the different numbers of Pt(II)---Pt(II) metal–metal bonds in host–guest complexation structures.

ARTICLE INFO

Article history:

Received 2 April 2019

Received in revised form 17 April 2019

Accepted 18 April 2019

Available online

ABSTRACT

Two host–guest systems have been constructed, by employing structurally similar terpyridine platinum(II) macrocycle and molecular tweezer as the synthetic receptors. The macrocycle/guest complex displays low-energy emission signal, reinforced non-covalent binding affinity, and enhanced photosensitization capability than those of the molecular tweezer/guest one. The discrepancy between macrocyclic and acyclic preorganization modes originates from the different numbers of Pt(II)---Pt(II) metal–metal bonds in host–guest complexation structures.

Keywords:

Supramolecular chemistry

Preorganization

Host–guest recognition

Preorganization is one of the key concepts in supramolecular chemistry field [1]. The common approach toward preorganization involves the fabrication of macrocyclic and molecular tweezer-like receptors, which limit the conformational degrees of freedom available [2, 3]. These rigid structures provide definite size and constrained environment for guest accommodation. For the resulting host–guest complexation system, a variety of non-covalent bonds can be incorporated in a multivalent and cooperative manner [4]. In this respect, we and others have constructed molecular tweezers and macrocycles with the presence of square-planar terpyridine platinum(II) units [5–7]. Thanks to the preorganization effect, these supramolecular receptors provide synergistic metal–metal and donor–acceptor interactions toward the complementary organometallic guests. The resulting host–guest systems are endowed with fascinating photo-physics and stimuli responsiveness, which are promising for biomedical and photo-catalytic applications [5d, 6f, 6i]. Despite the great progress achieved so far, it still requires deeper understanding of the preorganization effect, which facilitates to evaluate the contribution of non-covalent forces in a precise and quantitative manner.

Herein we have shown an interesting example, in which remarkable discrepancy exists between macrocyclic and acyclic preorganization modes [8]. Specifically, two structurally similar receptors **1–2** (Scheme 1) have been designed. Macrocyclic **1** preserves the basic structural feature of molecular tweezer **2**, while an extra C₁₀ alkyl linker is tethered between two terpyridine platinum(II) [Pt(II)(N[^]N[^]N)(C≡C–R)] units to achieve macrocyclization. Both **1** and **2** are capable of encapsulating neutral organoplatinum(II) [Pt(II)(C[^]N[^]C)(C≡N–R)] guest **3** (Scheme 1). Pt(II)---Pt(II) metal–metal forces are prone to form, because of the proximity of Pt(II) atoms between host and guest species. Unexpectedly, the subtle structural difference between **1** and **2** gives rise to huge difference on the number of Pt(II)---Pt(II) metal–metal bonds. In particular, two-fold Pt(II)---Pt(II) bonds are involved in macrocycle/guest complex **1/3**, while only one-fold bond exists for molecular tweezer/guest complex **2/3**. The optical properties, non-covalent binding strength, and photosensitization capability of the host–guest complexes can be further influenced by these two preorganization modes.

The designed macrocycle **1** and molecular tweezer **2** are synthesized quite straightforward (Schemes S1 and S2 in Supporting information). Both synthetic routes involve copper–catalyzed platinum–carbon coupling reactions as the final step. The identity and purity of **1–2** and the synthetic intermediates are unambiguously confirmed by means of ¹H, ¹³C NMR and ESI–MS spectra (Figs. S11–S25 in Supporting information). For **1** in chloroform, two absorbance bands are observed in the visible region ($\lambda_{\max} = 447$ nm and 472 nm, Fig. 1a). According to the previous literatures, they are assigned to MLCT/LLCT (metal–to–ligand and ligand–to–ligand charge transfer) transition of the [Pt(II)(N[^]N[^]N)(C≡C–R)] units [5a]. Moreover, MLCT/LLCT emission band of **1** is centred at 582 nm, together with a shoulder band at 620 nm (Fig. 1b). The large Stokes shift, along with the long lifetime in microsecond range ($\tau = 1.57$ μ s, Table S1 in Supporting information), illustrate the triplet origin of the MLCT/LLCT emission signals.

Remarkably, the MLCT/LLCT signals of **1** are bathochromic-shift than those of **2** (absorbance: $\lambda_{\max} = 425$ nm and 464 nm, emission: $\lambda_{\max} = 567$ nm, Figs. 1a and b). In view of the structural similarity between **1** and **2**, their distinct MLCT/LLCT spectroscopic signals are elucidated by means of DFT (density functional theory) calculations. For the optimized geometry of **1** (Fig. 1c) [9], the two [Pt(II)(N[^]N[^]N)(C≡C–R)] pincers are almost coplanar to each other, giving rise to the short Pt(II)---Pt(II) distance of 6.6 Å. In comparison, the two pincers on **2** are more twisted to form a V-shape conformation, accompanied by the long Pt(II)---Pt(II) distance of 10.9 Å (Fig. 1d). Meanwhile, the dihedral angle of the diphenylpyridine spacer varies from 15.5° for **1** to 30.7° for **2**. Hence, **1** possesses higher effective π -conjugation length than that of **2**, contributing to the bathochromic shifts of MLCT/LLCT signals.

Non-covalent complexation behaviors are further studied between the positively–charged receptors **1–2** and neutral guest **3**. For **3** itself, the intra-ligand (IL) absorption is located at 320–400 nm, while no emission signal can be observed (Fig. S1 in Supporting information) [10]. Upon mixing an equimolar amount of **1** and **3** together in CHCl₃, a low–energy absorbance appears between 520 and 640 nm (Fig. 2a), which is absent for the individual species. With reference to the previous reports [5a], the emergent band is characteristic for Pt(II)---Pt(II) MMLCT (metal–metal–to–ligand charge transfer) transitions. The phenomenon suggests the formation of non-covalent host–guest complex, leading to the proximity of heterologous Pt atoms between **1** and **3**. Although the MMLCT absorbance exists upon mixing **2** and **3** together (ranging from 520 to 620 nm, Fig. 2a), the extinction coefficient value of **2/3** is 3 times lower than that of **1/3** (at 550 nm, ϵ : 1.91×10^3 dm³ mol⁻¹ cm⁻¹ of **1/3**, versus 0.65×10^3 dm³ mol⁻¹ cm⁻¹ of **2/3**).

Moreover, the two host–guest complexes exhibit distinct emission properties (Fig. 2b). In particular, a near infrared MMLCT emission signal appears at 803 nm for **1/3**, accompanying by the severe quenching of MLCT/LLCT emission signal. On the contrary, the MMLCT emission intensity of **2/3** is significantly lower than that of the MLCT/LLCT signal derived from **2**. As a consequence, brown and green emission colours are visualized under 365 nm UV lamp for complexes **1/3** and **2/3**, respectively (Fig. 2b, inset).

To explain the intensive MMLCT signals in complex **1/3** than that of **2/3**, DFT theoretical calculations are further employed. As shown in Figs. 3a and b, guest **3** is encapsulated into the cavities of the host receptors for both complexes [9]. In terms of **1/3**, the interplanar distances between **3** and two [Pt(II)(N[^]N[^]N)(C≡C–R)] pincers on macrocycle **1** are calculated to be 3.45 Å and 3.46 Å, respectively (Fig. 3a). Simultaneously, intermolecular Pt(II)---Pt(II) distances are determined to be 3.49 Å and 3.42 Å, with the Pt–Pt–Pt angle of 172.6°. Hence, it is evident that both donor–acceptor and Pt(II)---Pt(II) metal–metal interactions exist in a two-fold manner. For molecular tweezer/guest complex **2/3**, it also possesses two-fold donor–acceptor forces, as manifested by the interplanar distances

of 3.57 Å and 3.47 Å. Nevertheless, the Pt(II)---Pt(II) distances are calculated to be 3.93 Å and 3.65 Å. The former one is too long to form Pt(II)---Pt(II) metal–metal bond. As a result, only one-fold metal–metal bond exists for **2/3**. Hence, it is evident that the number of Pt(II)---Pt(II) metal–metal bonds varies for the two preorganization modes.

Moreover, the quantitative binding thermodynamics are compared between **1/3** and **2/3**. For both complexes, the binding stoichiometries are determined to be 1:1, as manifested by the Job's plots on the basis of MMLCT absorbance intensity (Fig. 2c and Fig. S6 in Supporting information). The collected MMLCT absorbance at 555 nm is further fitted with one-site model (Eq. S1 in Supporting information), providing K_a value of $(7.86 \pm 1.33) \times 10^4 \text{ L mol}^{-1}$ for complex **1/3** (Fig. 2d). The value is determined to be $(8.93 \pm 0.19) \times 10^4 \text{ L mol}^{-1}$ on the basis of emission titration experiments (Fig. S3 in Supporting information). Besides, isothermal titration calorimetry (ITC) experiment provides an alternative method to quantify non-covalent binding affinity. Depending on the exothermic isotherm curve, K_a value of **1/3** is determined to be $(8.73 \pm 0.95) \times 10^4 \text{ L mol}^{-1}$ (Fig. 2e), which is consistent with the above spectroscopic titration results. Noteworthy, the K_a values of **1/3** are 16- and 9.4-fold higher than those of **2/3** ($K_{a,UV} = (4.93 \pm 0.03) \times 10^3 \text{ L mol}^{-1}$ and $K_{a,FL} = (9.52 \pm 0.01) \times 10^3 \text{ L mol}^{-1}$, Figs. S4 and S5 in Supporting information) on the basis of absorption and emission measurements, respectively.

The reinforced host–guest complexation strength from acyclic to macrocyclic preorganization are further validated *via* ^1H NMR experiments. For complex **1/3**, protons $\text{H}_{10,11}$ remain almost intact, while the terpyridine protons on **1** and the diphenylpyridine protons on **3** undergo enormously upfield shifts (−0.79, −0.61, −0.71, −1.00 and −0.94 ppm for H_1 , H_2 , H_3 , H_d , and H_e , respectively, Figs. S7a–c in Supporting information). It supports the presence of donor–acceptor interactions between the positively-charged $[\text{Pt}(\text{II})(\text{N}^+\text{N}^+\text{N})(\text{C}\equiv\text{C}-\text{R})]$ units on **1** and the neutral $[\text{Pt}(\text{II})(\text{C}^+\text{N}^+\text{C})(\text{C}\equiv\text{N}-\text{R})]$ unit on **3**. In comparison, complex **2/3** displays weaker host–guest complexation tendency, as reflected by the less upfield resonances shifts ($\Delta\delta = -0.38$ and -0.46 ppm for H_{d-e} , respectively, Fig. S7c–e in Supporting information).

As previously documented, the presence of long-lived triplet excited states renders excellent photosensitization capability to terpyridine platinum(II) complexes [11]. Upon formation of host–guest complexes **1/3** and **2/3**, the MMLCT transition signals emerge at the low-energy region, which facilitate photosensitization under the mild visible light conditions (Fig. 4a). In this regard, an OLED lamp (12 W, 590 nm) is employed, which overlaps with the MMLCT absorbance of host–guest complexes. Upon photo-irradiating **1/3** (0.05 mmol/L) and 9,10-dimethylantracene (DMA, 0.25 mmol/L) together in chloroform, the typical absorbance of DMA ($\lambda_{\text{max}} = 360, 380$ and 410 nm, Fig. 5b) decline for their intensities. The results suggest energy transfer between the triplet excited state of **1/3** and surrounding molecular oxygen (Fig. 4a). Singlet oxygen ($^1\text{O}_2$) formed *in situ* is further captured by DMA to form 9,10-dimethylantracene 9,10-endoperoxide, as verified by upfield shifting of the DMA methyl resonances from 3.22 ppm to 2.26 ppm (Fig. S9 in Supporting information).

The quantitative $^1\text{O}_2$ generation rate can be further acquired (Eq. S2 in Supporting information), which is $3461 \text{ min}^{-1} \text{ L mol}^{-1}$ for complex **1/3** (0.05 mmol/L for each compound, Fig. 4c). The value is significantly higher than those of the individual species (**1**: $171.4 \text{ min}^{-1} \text{ L mol}^{-1}$, **3**: $4.10 \text{ min}^{-1} \text{ L mol}^{-1}$, Fig. 4c and Fig. S10 in Supporting information). It is highly plausible, since the emergent MMLCT band is crucial for $^1\text{O}_2$ production under the visible light irradiation conditions. More intriguingly, $^1\text{O}_2$ generation capability of **1/3** is approximately 3-fold higher than that of **2/3** ($1209 \text{ min}^{-1} \text{ L mol}^{-1}$). Considering that both **1/3** and **2/3** are in dynamic equilibrium between complexed (the real photosensitization species) and uncomplexed states, the different photosensitization capabilities for **1/3** and **2/3** are rationalized *via* the mathematical calculation (Eq. S3 in Supporting information). In detail, 61% of the complexed species exist for **1/3** at the monomer concentration of 0.05 mM. In stark contrast, only 19% of **2/3** exists in the “active” complexed form. The results unambiguously support that, in addition to the emergent MMLCT absorbance, host–guest binding strength also exerts crucial impact on visible-light photosensitization efficiency.

In summary, subtle structural variation between macrocycle **1** and molecular tweezer **2** gives rise to the remarkable discrepancy in host–guest complexation behaviours. Although both donor–acceptor and Pt(II)---Pt(II) metal–metal interactions are involved in both **1/3** and **2/3**, these two complexes possess different numbers of Pt(II)---Pt(II) metal–metal bonds. As a result, **1/3** displays one order of magnitude higher for the non-covalent binding affinity, and 3-fold enhancement for the photosensitized $^1\text{O}_2$ generation capability than those of **2/3**. The prominent role of preorganization modes (macrocyclic *versus* acyclic) exemplified in the current work would benefit for the rational design of host–guest systems in future study.

Acknowledgments

This work was supported by the National Natural Science Foundation of China (Nos. 21674106 and 21871245), CAS Youth Innovation Promotion Association (No. 2015365), and the Fundamental Research Funds for the Central Universities (No. WK3450000004).

References

- [1] D.J. Cram, *Angew. Chem. Int. Ed.* 25 (1986) 1039–1057.
- [2] (a) J.M. Lehn, *Science* 260 (1993) 1762–1763.
- (b) F. Wang, J. Zhang, X. Ding, et al., *Angew. Chem. Int. Ed.* 49 (2010) 1090–1094.
- (c) M. Xue, Y. Yang, X. Chi, X. Yan, F. Huang, *Chem. Rev.* 115 (2015) 7398–7501.
- (d) Z. Liu, S.K.M. Nalluri, J.F. Stoddart, *Chem. Soc. Rev.* 46 (2017) 2459–2478.
- (e) K. Kotturi, E. Masson, *Chem. Eur. J.* 24 (2018) 8670–8678.
- (f) S. Kuang, Z. Hu, H. Zhang, et al., *Chem. Commun.* 54 (2018) 2169–2172.

- [3] (a) C.W. Chen, H.W. Whitlock, *J. Am. Chem. Soc.* 100 (1978) 4921–4922.
(b) S.C. Zimmerman, W. Wu, *J. Am. Chem. Soc.* 111 (1989) 8054–8055.
(c) M. Hardouin-Lerouge, P. Hudhomme, M. Salle, *Chem. Soc. Rev.* 40 (2011) 30–43.
(d) C. Shao, M. Stolte, F. Wuerthner, *Angew. Chem. Int. Ed.* 52 (2013) 7482–7486.
(e) S. Ibáñez, M. Poyatos, E. Peris, *Angew. Chem. Int. Ed.* 56 (2017) 9786–9790.
(f) Y. Han, Y. Tian, Z. Li, F. Wang, *Chem. Soc. Rev.* 47 (2018) 5165–5176.
(g) S. Ibáñez, M. Poyatos, E. Peris, *Angew. Chem. Int. Ed.* 57 (2018) 16816–16820.
- [4] (a) J.D. Badjic, A. Nelson, S.J. Cantrill, W.B. Turnbull, J.F. Stoddart, *Acc. Chem. Res.* 38 (2005) 723–732.
(b) C.A. Hunter, H.L. Anderson, *Angew. Chem. Int. Ed.* 48 (2009) 7488–7499.
(c) L.K.S. von Krbek, C.A. Schalley, P. Thordarson, *Chem. Soc. Rev.* 46 (2017) 2622–2637.
- [5] (a) Y. Tanaka, K.M.C. Wong, V.W.W. Yam, *Chem. Sci.* 3 (2012) 1185–1191.
(b) Y. Tanaka, K.M.C. Wong, V.W.W. Yam, *Angew. Chem. Int. Ed.* 52 (2013) 14117–14120.
(c) Y. Tanaka, K.M.C. Wong, V.W.W. Yam, *Chem. Eur. J.* 19 (2013) 390–399.
(d) A.K.W. Chan, W.H. Lam, Y. Tanaka, K.M.C. Wong, V.W.W. Yam, *Proc. Natl. Acad. Sci. U.S.A.* 112 (2015) 690–695.
(e) F.K.W. Kong, A.K.W. Chan, M. Ng, K.H. Low, V.W.W. Yam, *Angew. Chem. Int. Ed.* 56 (2017) 15103–15107.
- [6] (a) Y.K. Tian, Y.G. Shi, Z.S. Yang, F. Wang, *Angew. Chem. Int. Ed.* 53 (2014) 6090–6094.
(b) Y.K. Tian, Y.F. Yang, Z.S. Yang, F. Wang, *Macromolecules* 49 (2016) 6455–6461.
(c) Z. Gao, Y. Han, J. Chen, X. Wang, F. Wang, *Chem. Asian J.* 11 (2016) 1775–1779.
(d) X. Lv, Y. Han, Z. Yang, et al., *Tetrahedron Lett.* 57 (2016) 1971–1975.
(e) Z. Li, Y. Han, F. Jin, et al., *Daltron Trans.* 45 (2016) 17290–17295.
(f) Z. Li, Y. Han, Z. Gao, F. Wang, *ACS Catal.* 7 (2017) 4676–4681.
(g) T. Fu, Z. Li, Z. Zhang, X. Zhang, F. Wang, *Macromolecules* 50 (2017) 7517–7525.
(h) Z. G, Y. Han, S. Chen, et al., *ACS Macro Lett.* 6 (2017) 541–545.
(i) Z. Li, Y. Han, Z. Gao, T. Fu, F. Wang, *Mater. Chem. Front.* 2 (2018) 76–80.
(j) X. Zhang, L. Ao, Y. Han, Z. Gao, F. Wang, *Chem. Commun.* 54 (2018) 1754–1757.
(k) Z. Gao, Y. Han, Z. Gao, F. Wang, *Acc. Chem. Res.* 51 (2018) 2719–2729.
- [7] (a) A.J. Goshe, I.M. Steele, B. Bosnich, *J. Am. Chem. Soc.* 125 (2003) 4444–4450.
(b) J.D. Crowley, I.M. Steele, B. Bosnich, *Inorg. Chem.* 44 (2005) 2989–2991.
(c) Y. Yamaki, T. Nakamura, S. Suzuki, et al., *Eur. J. Org. Chem.* (2016) 1678–1683.
- [8] (a) D. Canevet, M. Gallego, H. Isla, et al., *J. Am. Chem. Soc.* 133 (2011) 3184–3190.
(b) J.M. McGrath, M.D. Pluth, *J. Org. Chem.* 79 (2014) 711–719.
- [9] To reduce the computational costs, the peripheral 4-butoxyphenyl groups on both **1** and **2** are removed during DFT calculation processes.
- [10] W. Lu, M.C. Chan, K.K. Cheung, C.M. Che, *Organometallics* 20 (2001) 2477–2486.
- [11] (a) D. Zhang, L.Z. Wu, L. Zhou et al., *J. Am. Chem. Soc.* 126 (2004) 3440–3441.
(b) Q.Y. Meng, T. Lei, L.M. Zhao, et al., *Org. Lett.* 16 (2014) 5968–5971.

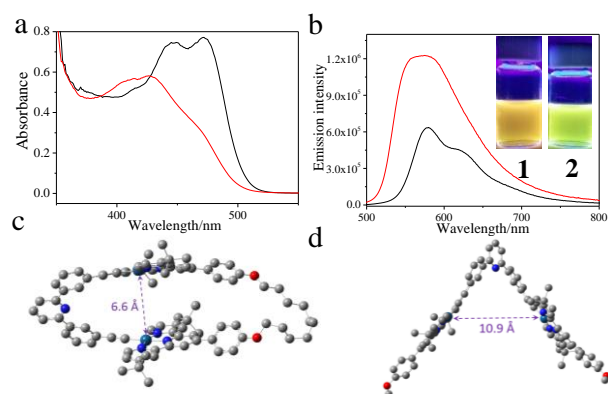


Fig. 1. (a) UV-vis spectra of **1** (black line) and **2** (red line) ($c = 0.25$ mmol/L in CHCl_3). (b) Emission spectra of **1** (black line) and **2** (red line) ($c = 0.10$ mmol/L in CHCl_3 , $\lambda_{\text{ex}} = 440$ nm). Inset of (b): images of **1** and **2** under 365 nm UV lamp. Optimized geometries of (c) **1**, and (d) **2** via DFT calculation. Pt atoms are described by LanL2dz, while the residual atoms are described by PBE/3-21G.

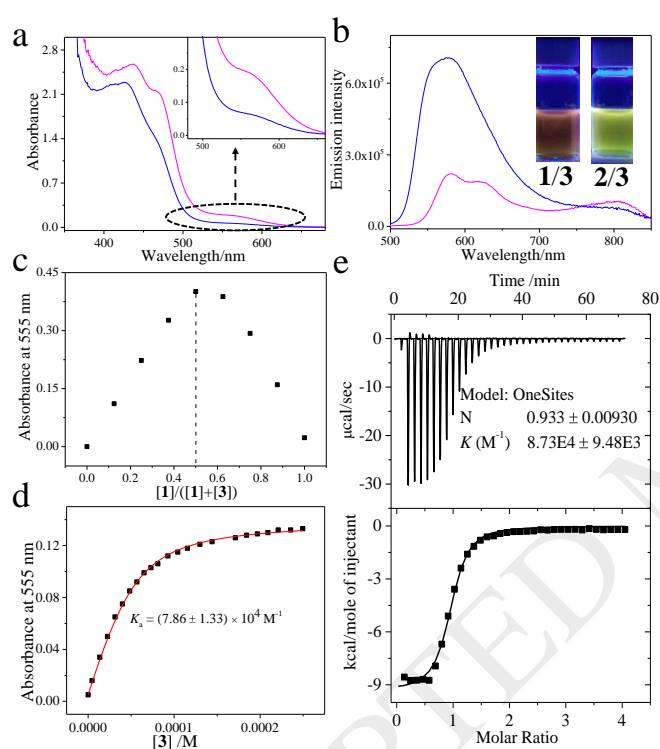


Fig. 2. (a) Absorption, and (b) emission spectra of **1/3** (pink lines) and **2/3** (blue lines) ($c = 0.10$ mmol/L for each compound in CHCl_3). Inset of (b): images of complexes **1/3** and **2/3** under 365 nm UV lamp. (c) Job's plot of **1/3**. (d) Intensity changes of MMLCT absorbance upon titrating **3** into the chloroform solution of **1** (0.05 mmol/L in CHCl_3). The red line denotes non-linear mathematical fitting. (e) ITC data by titrating **3** (8.00 mmol/L in CHCl_3 , 298 K) into the chloroform solution of **1** (0.40 mmol/L in CHCl_3).

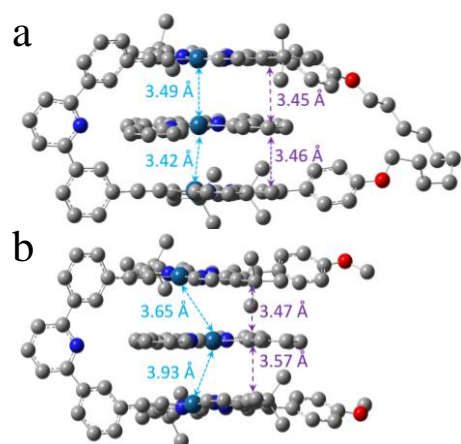


Fig. 3. Optimized structures of a) complex 1/3, and b) complex 2/3 *via* DFT calculation. Pt atoms are described by Lan12dz, while the residual atoms are described by PBE/3-21G.

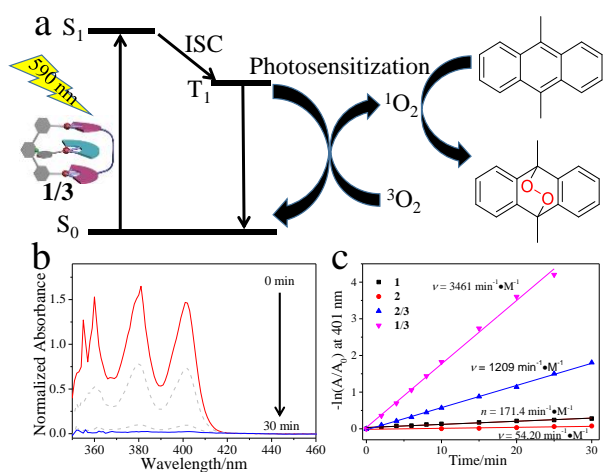
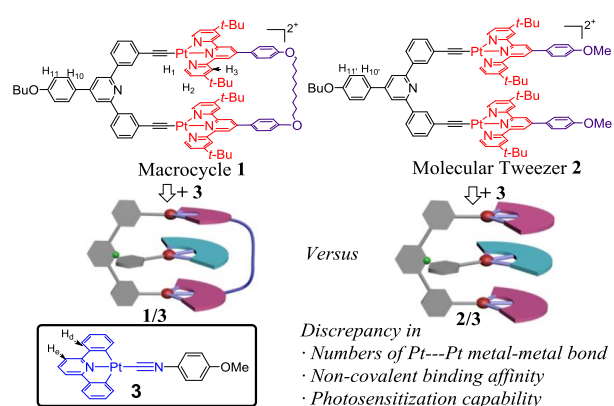


Fig. 4. (a) Schematic representation for the visible-light photosensitization process (ISC: intersystem crossing; ET: energy transfer). (b) UV-vis absorption changes of 9,10-dimethylanthracene (0.25 mmol/L in chloroform) upon light irradiation (590 nm, 12 W). Complex **1/3** ($c = 0.05$ mmol/L) is employed as the photosensitizer. (c) ¹O₂ generation efficiency of **1** (■), **2** (●), **2/3** (▲) and **1/3** (▼), by monitoring time-dependent absorbance of 9,10-dimethylanthracene at 401 nm.



Scheme 1. Schematic representation for the host-guest complexes **1/3** and **2/3**, by employing structurally similar macrocycle and molecular tweezer as the synthetic receptors. Triflate is served as the counterion in both **1** and **2**, which are omitted in the chemical structures.